Journal of Solid State Chemistry 183 (2010) 350–355

Contents lists available at ScienceDirect

Journal of Solid State Chemistry

journal homepage: www.elsevier.com/locate/jssc

Magnetic relaxation behavior of lanthanide substituted Dawson-type tungstoarsenates

Lizhen Liu, Fengyan Li, Lin Xu *, Xizheng Liu, Guanggang Gao

Key Laboratory of Polyoxometalate Science of Ministry of Education, Department of Chemistry, Northeast Normal University, Changchun, Jilin 130024, PR China

ARTICLE INFO

Article history:
Received 15 July 2009
Received in revised form
2 November 2009
Accepted 9 November 2009
Available online 13 November 2009

Keywords:
Crystal structure
Lanthanide
Tungstoarsenate
Magnetic properties
Cyclic voltammetry

ABSTRACT

Two new polyoxometalate compounds $[(CH_3)_4N]_8[Ln(H_2O)_8]_2[(\alpha_2\text{-}As_2W_{17}O_{61})Ln(H_2O)_2]_2\cdot nH_2O$ (*Ln*=Er (**1**), Dy (**2**)) have been prepared by the trivacant Dawson-type anion $[\alpha\text{-}As_2W_{15}O_{56}]^{12-}$ and trivalent rare earth ion and characterized by single-crystal X-ray diffraction, IR spectra, thermogravimetric and electrochemical analyses. The centrosymmetric polyoxoanion, $\{[(\alpha_2\text{-}As_2W_{17}O_{61})Ln(H_2O)_2]_2\}^{14-}$, bounded to each other via Ln^{3+} connecting to terminal W–O oxygen atoms. Furthermore, the polyoxoanions are linked by $[Ln(H_2O)_8]^{3+}$ to form an extensive 3D supramolecular network structure depending on hydrogen bond. The magnetic properties of the two compounds have been studied by measuring their magnetic susceptibilities in the temperature range 2.0–300.0 K, indicating the depopulation of the stark components at low temperature and/or very weak antiferromagnetic interactions between magnetic centers. Low-temperature ac magnetic susceptibility measurements reveal a slow magnetic relaxation behavior for **2**.

1. Introduction

Polyoxometalates (POMs), a class of metal oxygen clusters with fascinating structural variety and interesting properties have been attracting a great deal of attention as a result of their potential applications in catalysis, medicine and materials science [1–9]. It is well known that the lacunary POMs can be obtained by the removal of one or several metal centers and act as polydentate ligands. Lanthanide (*Ln*) cations, in virtue of their multiple coordination numbers and oxophilicity, are suitable to be incorporated into the lacunary POMs and link polyoxometalates to form new classes of materials with useful magnetic, luminescent properties, etc. [10–13].

Up to now, the two most studied polyoxometalate types have been the Keggin [14] and Well-Dawson [15] series, which are represented by $[XM_{12}O_{40}]^{n-}$ and $[X_2M_{18}O_{62}]^{n-}$ (X=P^V, Si^{IV}; M=$W^{V,VI}$, $Mo^{V,VI}$, $V^{IV,V}$), respectively. Since the first lanthanide complexes based on $[SiW_{11}O_{39}]^{8-}$ and $[P_2W_{17}O_{61}]^{10-}$ were prepared by Peacock and Weakley in 1971 [16], much attention has been focused on developing the polyoxometalate-based lanthanide complexes by incorporating the *Ln* ions into lacunary POMs. In particular, the monovancant Keggin polyoxometalates linked by Ln^{3+} have been elaborately investigated and some crystal structures have been determined [17–22]. For example, Pope et al. obtained the extended polymeric structures of the $Ln/[\alpha\text{-}SiW_{11}O_{39}]^{8-}$ (*Ln*=La^{III}, Ce^{III}) in 2000 [17]. Furthermore, Mialane et al. reported the solid state structures of $\{Ln_n(SiW_{11}O_{39})\}$ Polyoxoanions (*Ln*=Yb^{III}, Nd^{III}, Eu^{III}, Gd^{III}) in 2003 [18] and the dimeric $K_{12}[(SiW_{11}O_{39}Ln)_2(\mu\text{-}CH_3COO)_2]$ (*Ln*=Gd^{III}, Yb^{III}) complexes in 2004 [19].

In contrast, there are few reports about lanthanide complexes based on monovacant Dawson-type building block. The only examples are 1:1-type dimers of $[\{Ce(\alpha_1\text{-}P_2W_{17}O_{61})(H_2O)_4\}_2]^{14-}$ [23], $[\{Ln(\alpha_2\text{-}P_2W_{17}O_{61})(H_2O)_n\}_2]^{14-}$ (*Ln*=Ce, Eu, Nd) [24–26] as well as 1:2-type dimer of $[Lu(\alpha_2\text{-}P_2W_{17}O_{61})_2]^{17-}$ [27]. To our knowledge, the open angle of $[\alpha_2\text{-}As_2W_{17}O_{61}]^{10-}$ anion in the vacant site is larger than that of $[\alpha_2\text{-}P_2W_{17}O_{61}]^{10-}$, this is more favorable to accommodate various lanthanide cations for assembling the type of $Ln/[\alpha_2\text{-}As_2W_{17}O_{61}]^{10-}$ complexes with novel structures. Until recently, several *Ln*-containing tungstoarsenates, $(H_3O)[Ln_3(H_2O)_{17}(\alpha_2\text{-}As_2W_{17}O_{61})]\cdot nH_2O$, with one-dimensional chain structures, were reported by Zhao et al. [28]. Although the crystal structures of the *Ln*-POMs have been well studied in all previous reports, their magnetic properties are still rarely explored. In fact, the magnetic properties of lanthanide complexes closely depend on the coordination situation of Ln^{3+} ions, such as the coordination number, the kind of ligand atoms, bond angle, and bond length. As for lanthanide complexes, even a minor change of coordination situation could cause obvious alteration of magnetic properties. Therefore, the exploration of magnetic

* Corresponding author. Fax: +86 431 85099668.
E-mail address: linxu@nenu.edu.cn (L. Xu).

0022-4596/$ - see front matter © 2009 Elsevier Inc. All rights reserved.
doi:10.1016/j.jssc.2009.11.013

properties for polyoxometalate-based lanthanide complexes should be of considerable significance. In addition, our research demonstrated that the rational selection of solvents and counter-cations was a key factor to realize the successful synthesis.

Herein, we reported two new polyoxometalate-based lanthanide complexes assembled by lacunary Dawson-type anion $[\alpha_2\text{-}As_2W_{17}O_{61}]^{10-}$ and Ln^{3+} ions, $[(CH_3)_4N]_8[Er(H_2O)_8]_2[(\alpha_2\text{-}As_2W_{17}O_{61})Er(H_2O)_2]_2\cdot 26H_2O$ (**1**) and $[(CH_3)_4N]_8[Dy(H_2O)_8]_2[(\alpha_2\text{-}As_2W_{17}O_{61})Dy(H_2O)_2]_2\cdot 32H_2O$ (**2**). In particular, their magnetic properties were investigated in detail. These complexes were synthesized by reaction of the metastable, trivacant $[\alpha\text{-}As_2W_{15}O_{56}]^{12-}$ with the Ln^{3+} to form a $[(\alpha_2\text{-}As_2W_{17}O_{61})Ln(H_2O)_2]_2$ dimer. Furthermore, the dimers are linked by $[Ln(H_2O)_8]^{3+}$ to extend into a 3D supramolecular network structure in virtue of hydrogen bonds interaction. The static magnetic measurements on **1** and **2** reveal weak antiferromagnetic interactions between the *Ln* ions. Interestingly, the dynamic magnetic measurements for compound **2** display a slow relaxation of magnetization, showing a frequency-dependent susceptibility.

2. Experimental

2.1. General methods and materials

The $Na_{12}[\alpha\text{-}As_2W_{15}O_{56}]\cdot 21H_2O$ was prepared according to the literature [29] and confirmed by IR spectroscopy. The $ErCl_3\cdot 6H_2O$ was prepared by the reaction of Er_2O_3 and HCl. $DyCl_3\cdot 6H_2O$ was obtained by similar management. Other reagents were purchased commercially and used without further purification. The elemental analyses were determined by a Leaman inductively coupled plasma (ICP) spectrometer. The infrared spectra were obtained on an Alpha Centaurt FT/IR spectrometer with a pressed KBr pellet in the range of 400–4000 cm^{-1}. TG analyses were performed on a Perkin-Elmer TGA7 instrument in N_2 atmosphere with a heating rate of 10 °C min^{-1}. The magnetic susceptibility measurements for **1** and **2** were carried out using a Quantum Design MPMS-XL SQUID magnetometer at 1000 Oe. The ac susceptibility measurements were performed using an oscillating ac field of 3 Oe and ac frequencies ranging from 100 to 1500 Hz. Cyclic voltammetry measurements were carried out on a CHI 660 electrochemical workstation with a conventional three-electrode single compartment cell at room temperature. The working electrode was a glassy carbon disk electrode. The surface of the glass carbon electrode was polished with 0.3 and 0.05 μm Al_2O_3 powders successively, and washed with distilled water before each experiment. Platinum wire was used as counter electrode and SCE was used as reference electrode. The concentrations of **1** and **2** in the measurement of cyclic voltammetric behaviors were all 1.0×10^{-4} M.

2.2. Synthesis of $(CH_3)_4N]_8[Er(H_2O)_8]_2[(\alpha_2\text{-}As_2W_{17}O_{61})Er(H_2O)_2]_2\cdot 26H_2O$ **1**

$Na_{12}[\alpha\text{-}As_2W_{15}O_{56}]\cdot 21H_2O$ (0.054 g, 0.0125 mmol) was slowly dissolved in the hot (70 °C) solution containing 5 ml acetonitrile (CH_3CN) and 15 ml water with vigorous stirring. Then solid $ErCl_3\cdot 6H_2O$ (0.076 g, 0.2 mmol) was added. The resulting cloudy solution was heated at approximately 70 °C for 80 min. Then 0.1 g tetramethylammonium bromide was added and heated at the same temperature. After 40 min, the solution was cooled to room temperature, and the precipitate was removed by filtration. The filtrate was left to evaporate at room temperature for two days. Pink pillar-like crystals of **1**, suitable for X-ray diffraction, were collected. Yield: 0.02 g (35%, based on W). IR (KBr pellets, cm^{-1}): 3385(m), 951(m), 831(s), 778(s), 522(m). Elemental analyses calcd (%): W, 59.11; As, 2.83; Er, 6.33; C, 3.63; H, 1.77; N, 1.06. Found: W, 58.60; As, 2.79; Er, 6.21; C, 3.72; H, 1.85; N, 1.15.

2.3. Synthesis of $(CH_3)_4N]_8[Dy(H_2O)_8]_2[(\alpha_2\text{-}As_2W_{17}O_{61})Dy(H_2O)_2]_2\cdot 32H_2O$ **2**

The preparation procedure was the same as the preparation of complex **1** described above except that $DyCl_3\cdot 6H_2O$ was used (0.075 g). Yield: 0.017 g (30%, based on W). IR (KBr pellets, cm^{-1}): 3380(m), 952(m), 835(s), 777(s), 521(m). Elemental analyses calcd (%): W, 58.61; As, 2.81; Dy, 6.10; C, 3.60; H, 1.87; N, 1.05. Found: W, 58.01; As, 2.75; Dy, 5.97; C, 3.68; H, 1.94; N, 1.12.

2.4. Single crystal X-ray diffraction

Single-crystal data of compound **1** were collected on a Siemens SMARTCCD diffractometer with graphite-monochromated Mo*K*α (λ=0.71073 Å) radiation at 296 K. Single-crystal data of compound **2** were performed on a *R*-axis RAPID IP diffractometer equipped with a normal focus, 18 kW sealed-tube X-ray source (Mo KR radiation, λ=0.71073 Å) at 296 K. The structures were solved by direct methods and refined using full-matrix least-squares methods on F^2. All calculations were performed using the SHELX97 program package [30]. Empirical absorption corrections were applied. Parts of the non-hydrogen atoms were refined isotropically. The hydrogen atoms attached to the water molecules were not located in these compounds. The number of lattice water molecules for **1**,**2** are determined by thermal gravimetric (TG) and elemental analyses. Crystal data and structure refinement parameters for **1** and **2** are given in Table 1. Selected bond lengths and angles are list in supporting information.

Table 1
Crystal data and structure refinement for **1** and **2**.

1	**2**	
Empirical formula	$C_{32}H_{186}N_8Er_4O_{167}As_4W_{34}$	$C_{32}H_{198}N_8Dy_4O_{173}As_4W_{34}$
F_w	10 575.06	10 664.11
CityplaceCrystal system	Triclinic	Triclinic
Space group	*P*-1	*P*-1
a (Å)	13.2330(10)	13.239(3)
b (Å)	18.2319(14)	18.267(4)
c (Å)	19.9859(15)	20.032(6)
α (deg)	93.5150(10)	93.421(9)
β (deg)	97.6350(10)	97.625(9)
γ (deg)	96.8940(10)	96.903(7)
V (Å^3)	4729.9(6)	4753(2)
Z	1	1
D_{calcd} (g cm^{-3})	3.667	3.643
T (K)	296(2)	296(2)
λ (Å)	0.71073	0.71073
limiting indices	$-15\le h\le 16$	$-16\le h\le 15$
	$-21\le k\le 22$	$-22\le k\le 21$
	$-24\le l\le 17$	$-24\le l\le 24$
θ range (deg)	1.03–25.60°	3.09–25.60°
Data/restraints/ parameters	17 522/14/1044	16 838/2/949
Data collected/unique	25 367/17 522	36 289/16 838
Refinement method	F^2	F^2
Goodness of fit on F^2	1.033	1.027
Final R_1, $\omega R_2[I>2\sigma(I)]$	0.0465, 0.1114	0.0549, 0.1247
Final R_1, ωR_2 (all data)	0.0734, 0.1300	0.0964, 0.1461

Note. $R_1=\sum||F_o|-|F_c||/\sum|F_o|$, $wR_2=\{\sum[w(F_o^2-Fc^2)^2]/[\sum w(Fo^2)^2]\}^{1/2}$.

3. Results and discussion

3.1. Synthesis

Two lanthanide complexes were obtained using the similar synthetic procedure by reaction of the Ln^{3+} cations with the trivacant, metastable $[\alpha\text{-}As_2W_{15}O_{56}]^{12-}$ polyoxoanions. It is not entirely expected that we obtained the monolacunary Dawson-type fragment in our product. Considering that the reaction was approximately carried out at pH=4–5 and 70 °C, the $[\alpha\text{-}As_2W_{15}O_{56}]^{12-}$ may not be stable in acidic medium and rearranges slowly to the more stable $[\alpha_2\text{-}As_2W_{17}O_{61}]^{10-}$ [31]. It was well known that the conventional solution synthesis is a favorable method for succedent crystal growth. In the conventional synthesis process, different factors can affect the product formation and succedent crystal growth, such as selection of solvent, pH values, reaction time, and temperature. In our experiments, the rational selection of solvent was a key factor for the crystallization of products. The two title compounds could not be obtained in water. However, they were synthesized in mixed solvents of acetonitrile and water system, where the single crystals produced only in two days. The crystallized time is shorter than that of the previously reported compounds [28].

3.2. Structure description

X-ray diffraction analysis reveals that the solid-state structures of compounds **1**,**2** are isomorphic. Therefore, the following structural discussion is solely exemplified on the basis of compound **1**. It is built on monovacant Dawson-type polyoxoanions $[\alpha_2\text{-}As_2W_{17}O_{61}]^{10-}$ and Ln^{3+} ions. The $[\alpha_2\text{-}As_2W_{17}O_{61}]^{10-}$ polyanion is obtained by removal of a $[WO]^{4+}$ unit from a "cap" WO_6 polyoxoanion of the parent anion $[\alpha\text{-}As_2W_{18}O_{62}]^{6-}$ formed of 18{WO_6} octahedra. The As–O bond distances are in the range of 1.659(10)–1.694(10) Å. The W–O bond distances vary between 1.695(11) and 2.366(10) Å and the O–W–O bond angles are within 71.7(4)–173.4(5)°.

The structure of **1** is composed of two $[(\alpha_2\text{-}As_2W_{17}O_{61})Er(H_2O)_2]^{7-}$ polyoxoanions, two discrete $[Er(H_2O)_8]^{3+}$, eight $[(CH_3)_4N]^+$ and several isolated crystal water molecules. The polyoxoanion $[(\alpha_2\text{-}As_2W_{17}O_{61})Er(H_2O)_2]^{7-}$ is based on the well-known PlaceTypePlaceTypeDawson structure of the $[\alpha\text{-}As_2W_{18}O_{62}]^{6-}$ with one W atom substituted by a Er atom. As shown in Fig. 1, the structure of **1** is a centrosymmertric dimer in a head to cap fashion built from two $[(\alpha_2\text{-}As_2W_{17}O_{61})Er(H_2O)_2]^{7-}$ fragments by means of two Er–O–W link. The Er1 cation occupies the vacant site of the $[\alpha_2\text{-}As_2W_{17}O_{61})]^{10-}$ subunit and it is seven-coordinated, four basic oxygen atoms (O20, O31,O35, O51) surround the vacant site of the lacunary anion, one terminal oxygen atom (O37) of the other $[(\alpha_2\text{-}As_2W_{17}O_{61})Er(H_2O)_2]^{7-}$ moiety and two water molecules (OW1,OW2). The structure is similar to $[Ce_2((H_2O)_6(\alpha_2\text{-}As_2W_{17}O_{61})_2]^{14-}$ [28]. Due to the smaller size of Er^{3+} than Ce^{3+}, it is reasonable that only two water molecules are coordinated to the Er^{3+} rather than three water molecules that are found coordinated to Ce^{3+}. Moreover, compared with $[Nd((H_2O)_3(\alpha_2\text{-}As_2W_{17}O_{61})]^{7-}$ [28], the As–Er distance (4.121 Å) is much shorter than the As–Nd distance (4.417 Å), may resulting from the larger "bite angle" of polyoxoanion $[\alpha_2\text{-}As_2W_{17}O_{61})]^{10-}$ and smaller radius of heavy rare earth ions Er^{3+} than light rare earth ions Nd^{3+}. In addition, the use of tetramethylammonium cations $[(CH_3)_4N]^+$ as countercations can influence on the structural of crystal products. There is a structural difference in that the previously studied compounds $(H_3O)[Ln_3(H_2O)_{17}(\alpha_2\text{-}As_2W_{17}O_{61})]\cdot nH_2O$ [28] is 1D polymer, whereas the compound **1** is centrosymmetric dimers. The difference may be caused by the following reasons. The 1:1-type *Ln*POM dimers can be linked into a 1D chainlike structure by using K^+ counterions as linker [32]. Because of a competition between the K^+ and Ln^{3+}, it is important to eliminate the interference of K^+ ions during the preparation of 1D polymer. In our reaction system, the surface of anionic clusters $[Ln_2(H_2O)_6(\alpha_2\text{-}As_2W_{17}O_{61})_2]^{14-}$ can not be binded by the large organic counterions $[(CH_3)_4N]^+$ to form ion pairs [32] but be surrounded by $[(CH_3)_4N]^+$ to form a separate dimer. In result, the Ln^{3+} ions could not link the dimers into 1D chain structure.

The bond lengths from Er(III) to the oxygen atoms of the polyoxometalate framework are in the range of 2.247(11)–2.271(10) Å. The bond distances between the Er(III) and the two water molecules are 2.369(11)–2.406(12) Å. The Er–O (oxygen atom of a terminal Wd=O) bond length is 2.313(11) Å. The disordered Er(2) cations are coordinated with eight water molecules. The Er–OW bond distances range from 2.331(19) to 2.379(12) Å.

It is noteworthy that oxygen atoms of polyanions are connected with the oxygen atoms from ligand water molecules coordinated to the discrete Er atoms by strong hydrogen bonding interactions with bond lengths in the range of 2.63–2.81 Å. As viewed from the polyhedral diagram along *a* axis (Fig. S1), the polyanions are linked by OW7···O33 and OW4···O56 to generate a one-dimensional linear chain. In the *bc*-plane, they are connected with OW8···O55, OW9···O7 and OW8···O52 (see Figs. S2 and S3). The extensive hydrogen bonds can stabilize both polyanions and the cations, and lead to the formation of a 3D supramolecular network structure between the chains as shown in Fig. S4.

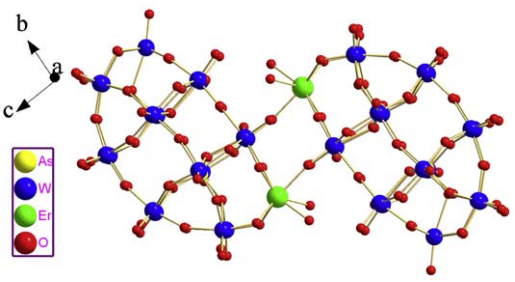

Fig. 1. Ball and stick structure of **1**. The hydrogen atoms, discrete Er^{3+} coordination ions, lattice water molecules and $[(CH_3)_4N]^+$ are omitted for clarity.

3.3. FT-IR spectroscopy

The IR spectra of two compounds share similarly characteristic vibrational features to other Dawson-type structures [28] as shown in Figs. S5 and S6. Asymmetric stretching vibrations of the different W–O bonds are observed as follows: 952 cm^{-1} (**1**) and 951 cm^{-1} (**2**) for terminal W–Od; 865 cm^{-1} (**1**) and 866 cm^{-1} (**2**) for W–Ob (Ob intrabridges between corner-sharing octahedra); the W–Oc (Oc intrabridges between edge-sharing octahedra) peak splits into two peaks: 778, 689 cm^{-1} (**1**) and 777, 690 cm^{-1} (**2**), these results show that the polyoxoanions of compounds **1**,**2** have lower symmetry than that of $[\alpha\text{-}As_2W_{18}O_{62}]^{6-}$ (D_{3h}) by removing a $[WO]^{4+}$ unit. Compared with the As–O bands of Well-Dawson polyoxoanion $[\alpha\text{-}As_2W_{18}O_{62}]^{6-}$, only one absorption peak could be observed at 835 cm^{-1}, but the other peak at 865 cm^{-1} is overlapped by the strong peak of W–Ob. A broad band at 3385 cm^{-1} (**1**) and 3380 cm^{-1} (**2**) associated with the aqua ligands. Additionally, a series of characteristic bands for the $[(CH_3)_4N]^+$ group are 1624, 1482, 1446, 1416, 1286 cm^{-1} in compound **1** and 1623, 1483, 1449, 1415, 1285 cm^{-1} in compound **2**.

3.4. Thermal analysis

The thermal gravimetric (TG) curve of compound **1** is shown in Fig. S7. It exhibits a total weight loss of 13.2% in the range of 26–480 °C, which agrees with the calculated value of 13.3%. In the range of 26–100 °C, consecutive three-step weight losses were observed with total weight loss of 4.5% corresponding to the loss of 25 free water molecules (calcd 4.3%). The weigh loss of 3.1% at 100–250 °C corresponds to the release of 20 coordination water with Er (calcd 3.4%). The last stage, which occurs from 250 to 480 °C, is attributed to the loss of eight $[(CH_3)_4N]^+$. The observed weight loss (5.6%) is in agreement with the calculated value (calcd 5.6%).

The TG curve of compound **2** is shown in Fig. S8. It exhibits a total weight loss of 14.28% in the range of 26–480 °C, which agrees with the calculated value of 14.18%. In the range of 26–100 °C, consecutive three-step weight losses were observed with total weight loss of 5.2% corresponding to the loss of 31 free water molecules (calcd 5.24%). The consecutive three-step weigh loss of 3.4% at 100–240 °C corresponds to the loss of 20 coordination water molecules with Dy (calcd 3.38%). Then, the weight loss of 5.6% at 240–480 °C corresponds to the loss of all $[(CH_3)_4N]^+$ (8 $[(CH_3)_4N]^+$, calcd 5.56%).

3.5. Magnetic properties

The magnetic behaviors of **1** are shown as plots of the product χ_m versus T and χ_mT versus T in Fig. 2. The χ_m value increases from 0.15 $cm^3\,mol^{-1}$ at 300 K, reaching a maximum of 15.12 $cm^3\,mol^{-1}$ at about 2 K as the temperature decreases. The value of χ_mT at room temperature is 46.02 $cm^3\,mol^{-1}$ K, which is close to the calculated value (45.92 $cm^3\,mol^{-1}$ K) for four non-interacting Er(III) in the $^4I_{15/2}$ ground state. Upon cooling, the value of χ_mT remains almost constant until at about 135 K when it decreases continuously and reaches 30.09 $cm^3\,mol^{-1}$ K at 2 K. The $1/\chi_m$ versus T plot could be fit with Curie–Weiss law from 50 to 300 K, getting C=46.5 $cm^3\,mol^{-1}$ K and θ=−2.67 K (Fig. S9). The decrease in χ_mT and the negative value of θ might be due to the progressive depopulation of the stark components of $^4I_{15/2}$ ground state of Er(III) ion and/or the weak antiferromagnetic interaction between the neighboring Er(III) ions [33].

Similar magnetic behavior to **1** was also revealed for **2** (Fig. 3). The χ_mT value at room temperature is 59.05 $cm^3\,mol^{-1}$ K, which is higher than the value of 56.72 $cm^3\,mol^{-1}$ K expected for four Dy(III) ion, including the significant contribution of 4*f* orbital

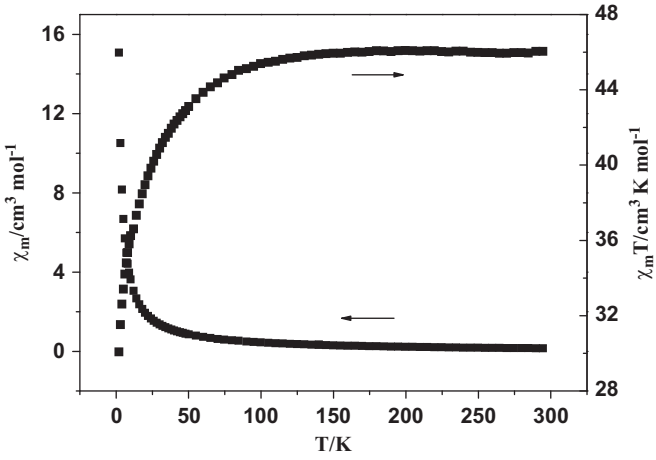

Fig. 2. Temperature dependence of χ_m and χ_mT for **1** at 2–300 K.

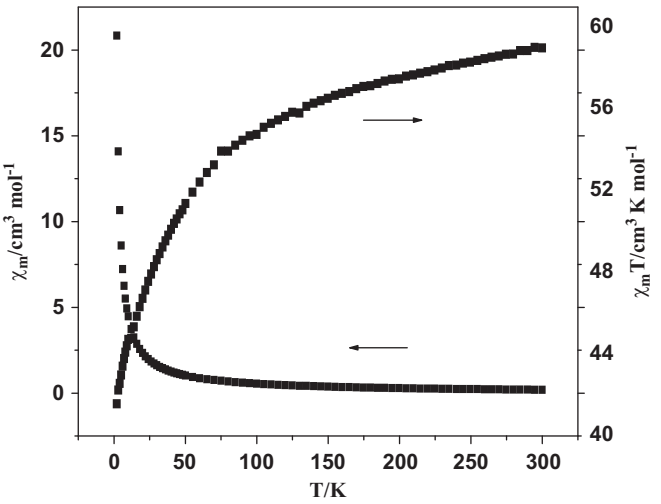

Fig. 3. Temperature dependence of χ_m and χ_mT for **2** at 2–300 K.

($4f^{10}$, $J=\frac{15}{2}$, $S=\frac{5}{2}$, $L=5$, $g=\frac{4}{3}$, $^6L_{15/2}$) [34]. As the temperature decreases, the value of χ_mT continuously decreases to 41.58 $cm^3\,mol^{-1}$ K at 2 K. The plot of $1/\chi_m$ versus T in the temperature range 50–300 K obeys the Curie–Weiss law with C=60.79 $cm^3\,mol^{-1}$ K and θ=−10.63 K (Fig. S10). All of these results indicate that there is a possible weak antiferromagnetic interaction between the neighboring Dy(III) ions and/or the crystal field effects on the Dy(III) Stark sub-levels, similar to other Dy(III) compounds [35].

It is well known that by electronic repulsion interaction and spin–orbit coupling, the $4f^n$ configuration of a Ln^{III} ion is split into $^{2S+1}L_J$ states. The crystal-field perturbation further leads to the splitting into Stark components. At room temperature, the Stark levels are entirely populated. While the temperature decreases, a gradual depopulation of these levels takes place [36]. To investigate the magnetic properties in detail, the temperature dependence of the alternating current (ac) magnetic susceptibility for compounds **1** and **2** was thus measured in a zero dc field in the range of 2–15 K at different frequencies (100–1500 Hz). No out-of-phase component of ac magnetic susceptibility χ_m was observed above 2 K for **1** (Fig. S11). Fig. 4 shows the temperature dependence of the ac magnetic susceptibility for **2**. A clearly frequency-dependent out-of-phase component was observed, but no Arrhenius plot can be extracted from this measurement, since no peak was observed in the χ_m versus T curves.

To study the thermal relaxation, a small dc field could be applied to remove the degeneracy of the m_s states connected by the tunnelling mechanism [35,37]. Therefore, the ac susceptibility measurements were carried out in a 3 Oe ac field oscillating at 100–1500 Hz, under a 1000 Oe static field. In the presence of a static magnetic field, remarkable changes were observed. The out-of-phase susceptibilities of the two compounds are all frequency-dependent, though the maxima of χ_m for **1** cannot be observed (Fig. S12). However, the maxima of both χ_m' and χ_m'' (Fig. 5) appeared for compound **2,** indicating a slow magnetic relaxation behavior. Analysis of the frequency dependence of the χ_m'' peaks through an Arrhenius plot ($\tau=\tau_0\exp(\Delta/k_BT)$) permits estimation of the energy barrier and the characteristic relaxation time in compound **2**. Best fitting (R=0.991) afforded a barrier height (Δ/k_B) of 11.8 K and a pre-exponential factor (τ_0) of 1.4×10^{-6} s (Fig. S13). Because the complexity of the ligand field energy levels for lanthanide complexes leads to the lack of suitably theoretical models, more detailed calculations of the magnetic interactions for **1** and **2** have to be limited in the present status.

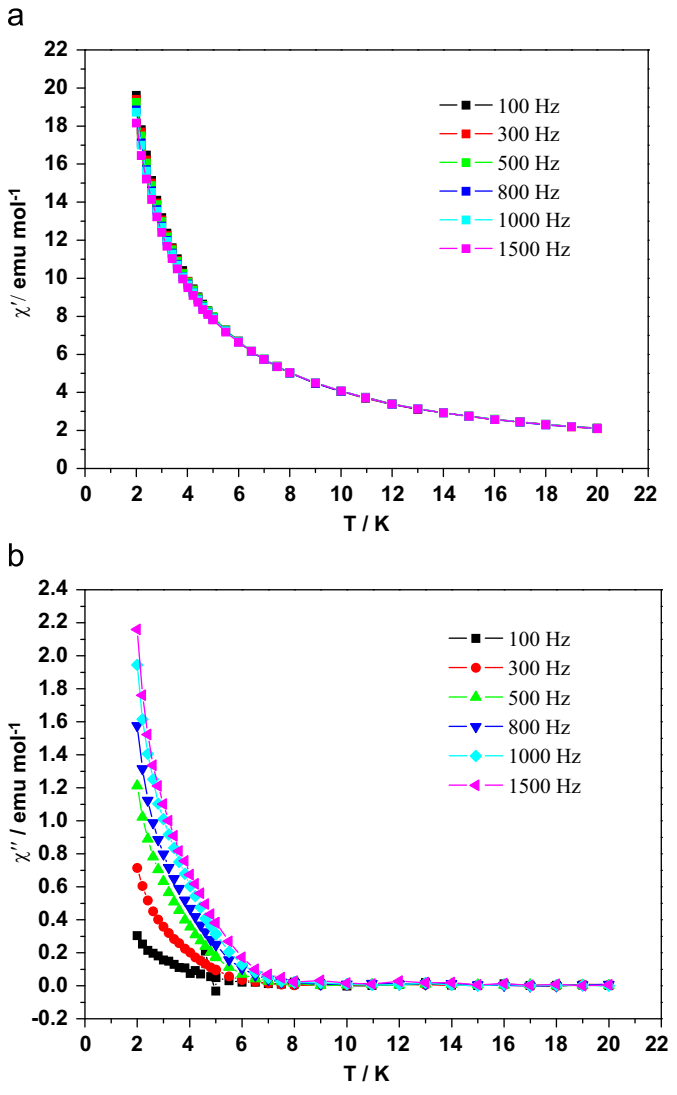

Fig. 4. Plot of the χ_m' (**a**) and χ_m'' (**b**) vs. T for **2**, where χ_m' and χ_m'' are in-phase ac and out-of-phase ac magnetic susceptibilities, respectively, measured with a 3 Oe ac magnetic field oscillating at the indicated frequencies in a zero applied static field.

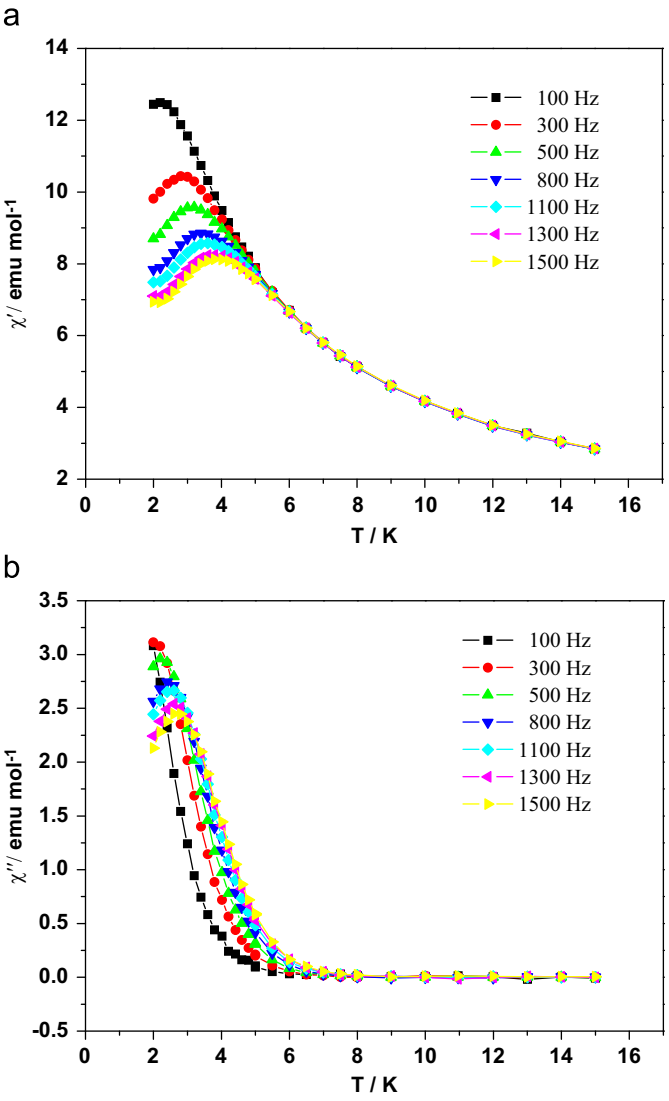

Fig. 5. Temperature dependence of the χ_m' (**a**) and χ_m'' (**b**) components of the ac susceptibility in a dc field of 1000 Oe with a 3 Oe ac magnetic field oscillating at the indicated frequencies for **2**.

3.6. Cyclic voltammetry behavior

Cyclic voltammetry (CV) of **1** were carried out in 0.5 M NaAc/HAc buffer solution at pH=4.3. The three redox processes ascribed to the oxo-tungsten framework are observed in the range of −1.1 to 0.4 V. The three redox couples correspond to one one-electron redox process followed by two two-electron redox processes. No redox wave on lanthanide ions is observed even if the potential range from +0.8 to −1.1 V, which is similar to the redox processes of $[Ln(As_2W_{17}O_{61})_2]^{17-}$ [38]. The CVs of **1** in pH=4.3 acetate buffers at different scan rates is shown in Fig. 6, consistent with that of the $[Ln(As_2W_{17}O_{61})_2]^{17-}$ [38]. When the scan rate is varying from 100 to 400 mV s^{-1}, the peak currents of **1** are almost proportional to it, taking the second redox peak as representative (inset of Fig. 6). This indicates that the redox waves are surface-controlled redox processes.

Compound **2** shows similar electron transfer processes as **1**. The three redox waves correspond to one- and two-electron transfer processes, respectively. The electrode reaction process of **2** is also surface-controlled, the same as compound **1** (Fig. S14).

4. Conclusions

In summary, two new lanthanide substituted Dawson-type tungstoarsenates $[(CH_3)_4N]_8[Er(H_2O)_8]_2[(\alpha_2\text{-}As_2W_{17}O_{61})Er(H_2O)_2]_2 \cdot 26H_2O$ and $[(CH_3)_4N]_8[Dy(H_2O)_8]_2[(\alpha_2\text{-}As_2W_{17}O_{61})Dy(H_2O)_2]_2 \cdot 32H_2O$ have been synthesized by interaction of the metastable, trivacant $[\alpha\text{-}As_2W_{15}O_{56}]^{12-}$ with the Ln^{3+}. The selection of solvent and counterions could influence on the formation of crystals and their structures. In addition, magnetic studies revealed that the weak antiferromagnetic interactions appear in the two complexes. The dynamic magnetic measurements show that compound **2** presents a slow magnetic relaxation behavior. Further work will focus on the rational adjustment of synthetic condition to isolate multinuclear polyoxometalate-based lanthanide complexes with diverse coordination geometry.

Supplementary materials

Structural figures, IR, TG, magnetic data, electrochemical properties and crystallographic data for compounds **1** and **2** are presented.

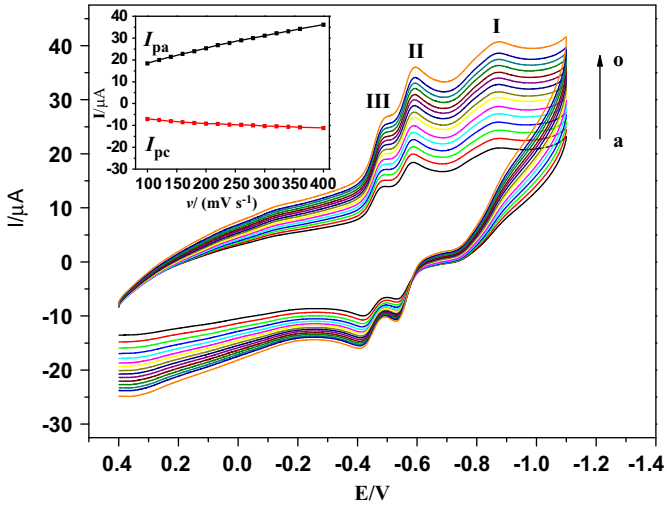

Fig. 6. Cyclic voltammograms of **1** in 0.5 M NaAc/HAc (pH=4.3) at different scan rates of (a) 100, (b) 120, (c) 140, (d) 160, (e) 180, (f) 200, (g) 220, (h) 240, (i) 260, (j) 280, (k) 300, (l) 320, (m) 340, (n) 360, and (o) 400 m V s^{-1}, respectively. Inset: the relationship of the scan rates vs. the second oxidation and reduction peak currents of W-centered redox reaction.

Crystallographic dates for the structure of the compounds reported in this paper have been deposited in the Cambridge Crystallographic Date center as supplementary publication number CCDC 695225 and 695226. Copies of the data can be obtained free of charge on application to The Director, CCDC, 12 Union Road, Cambridge CB21EZ, UK (Fax: +44 1223 336 033; E-mail: deposit@ccdc.cam.ac.uk).

Acknowledgments

The authors are thankful for the financial support from the Natural Science Foundation of China (Grant nos. 20671017 and 20731002) and the Program for Changjiang Scholars and Innovative Research Team in University. This work was also supported by Science Foundation for Young Teachers of Northeast Normal University (Grant no. 20090403).

Appendix A. Supplementary material

Supplementary data associated with this article can be found in the online version at 10.1016/j.jssc.2009.11.013.

References

[1] N. Mizuno, M. Misono, Chem. Rev. 98 (1998) 199–277.
[2] C.L. Hill, Angew. Chem. Int. Ed. 43 (2004) 402–404.
[3] J.T. Rhule, C.L. Hill, D.A. Judd, Chem. Rev. 98 (1998) 327–358.
[4] C.L. Hill, C.M. Prosser-McCartha, Coord. Chem. Rev. 143 (1995) 407–455.
[5] E. Coronado, C.J. Gómez-García, Chem. Rev. 98 (1998) 273–296.
[6] D.L. Long, E. Burkholder, L. Cronin, Chem. Soc. Rev. 36 (2007) 105–121.
[7] T.B. Liu, E. Diemann, H. Li, A. Dress, A. Müller, Nature 426 (2003) 59–62.
[8] T.B. Liu, J. Am. Chem. Soc. 125 (2003) 312–313.
[9] C. Fleming, D.L. Long, N. Mcmillan, J. Johnston, N. Bovet, V. Dhanak, N. Gadegaard, P. Kögerler, L. Cronin, M. Kadodwala, Nature. Nanotechnology. 3 (2008) 229–233.
[10] C. Benelli, D. Gatteschi, Chem. Rev. 102 (2002) 2369–2388.
[11] T. Yamase, Chem. Rev. 98 (1998) 307–325.
[12] J. Jing, B.P. Burton-Pye, L.C. Francesconi, M.R. Antonio, Inorg. Chem. 47 (2008) 6889–6899.
[13] C. Boglio, B. Hasenknopf, G. Lenoble, P. Rémy, P. Gouzerh, S. Thorimbert, E. Lacôte, M. Malacria, R. Thouvenot, Chem. Eur. J. 14 (2008) 1532–1540.
[14] J.F. Keggin, Nature 131 (1933) 908–909.
[15] B. Dawson, Acta Crystallogr. 6 (1953) 113–126.
[16] R.D. Peacock, T.J.R. Weakly, J. Chem. Soc. A. (1971) 1836–1839.
[17] M. Sadakane, M.H. Dickman, M.T. Pope, Angew. Chem. Int. Ed. 39 (2000) 2914–2916.
[18] P. Mialane, L. Lisnard, A. Mallard, J. Marrot, E. Antic-Fidancev, P. Aschehoug, D. Vivien, F. Se'écheresse, Inorg. Chem. 42 (2003) 2102–2108.
[19] P. Mialane, A. Mallard, E. Dolbecq, J. Marrot, F. Sécheresse, Eur. J. Inorg. Chem. (2004) 33–36.
[20] J.P. Wang, J.W. Zhao, X.Y. Duan, J.Y. Niu, Cryst. Growth Des. 6 (2006) 507–513.
[21] J.P. Wang, X.Y. Duan, X.D. Du, J.Y. Niu, Cryst. Growth. Des. 6 (2006) 2266–2270.
[22] L.H. Fan, L. Xu, G.G. Gao, F.Y. Li, Z.K. Li, Y.F. Qiu, Inorg. Chem. Commun. 9 (2006) 1308–1311.
[23] M. Sadakane, M.H. Dickman, M.T. Pope, Inorg. Chem. 40 (2001) 2715–2719.
[24] M. Sadakane, A. Ostuni, M.T. Pope, J. Chem. Soc., Dalton Trans. (2002) 63–67.
[25] Q.H. Luo, R.C. Howell, J. Bartis, M. Dankova, W.D. Horrocks Jr., A.L. Rheingold, L.C. Francesconi, Inorg. Chem. 41 (2002) 6112–6117.
[26] U. Kortz, J. Clust. Sci. 14 (2003) 205–214.
[27] Q.H. Luo, R.C. Howell, M. Dankova, J. Bartis, C.W. Williams, W.D. Horrocks Jr., V.G. Young Jr., A.L. Rheingold, L.C. Francesconi, M.R. Antonio, Inorg. Chem. 40 (2001) 1894–1901.
[28] X.Y. Zhao, S.X. Liu, Y.H. Ren, J.F. Cao, R.G. Cao, K.Z. Shao, J. PlaceTypePlace-TypeSolid PlaceTypeState Chem. 181 (2008) 2488–2493.
[29] L.H. Bi, E.B. Wang, J. Peng, R.D. Huang, L. Xu, C.W. Hu, Inorg. Chem. 39 (2000) 671–679.
[30] G.M. Sheldrick, SHELXTL-97, Programs for Crystal Structure Refinement, PlaceTypeUniversity of Göttingen, Germany, 1997.
[31] R. Contant, Inorg. Synth. 27 (1990) 108–111.
[32] C. Zhang, R.C. Howell, K.B. Scotland, F.G. Perez, L. Todaro, L.C. Francesconi, Inorg. Chem. 43 (2004) 7691–7701.
[33] J.C. Muñoz, A.M. Atria, R. Baggio, M.T. Garland, O. Peña, C. Orrego, Inorg. Chim. Acta. 358 (2005) 4027–4033.
[34] Z.H. Zhang, Y. Song, T. Okamura, Y. Hasegawa, W.Y. Sun, N. Ueyama, Inorg. Chem. 45 (2006) 2896–2902.
[35] M. Ferbinteanu, T. Kajiwara, K.Y. Choi, H. Nojiri, A. Nakamoto, N. Kojima, F. Cimpoesu, Y. Fujimura, S. Takaishi, M. Yamashita, J. Am. Chem. Soc. 128 (2006) 9008–9009.
[36] F.Y. Li, L. Xu, G.G. Gao, L.H. Fan, B. Bi, Eur. J. Inorg. Chem. (2007) 3405–3409.
[37] V. Chandrasekhar, B.M. Pandian, R. Boomishankar, A. Steiner, J.J. Vittal, A. Houri, R. Clérac, Inorg. Chem. 47 (2008) 4918–4929.
[38] X.D. Xi, G. Wang, B.F. Liu, S.J. Dong, Electrochim. Acta. 40 (1995) 1025–1029.